Micro/Nanotechnology for Picosatellites

Siegfried W. Janson
The Aerospace Corporation
Mail Stop M2/241, P.O. Box 92957, Los Angeles, CA 90009-2957; 310.336.7420
Siegfried.w.janson@aero.org

ABSTRACT

Up until the year 2000, only a few active picosatellites had been put into orbit. For the first 40 years of the Space Age, it was difficult to integrate high levels of functionality into the picosatellite 0.1 to 1-kg mass range. Fortunately, continuing advancements in micro/nanoelectronics and microelectromechanical systems has now enabled many nanosatellite and microsatellite capabilities to be implemented in picosatellites. Complementary metal oxide semiconductor (CMOS) micro/nanoelectronics are currently mass-produced with lateral structures smaller than 65-nm, thus enabling creation of billion-transistor integrated circuits on cm-scale silicon dice. Microelectromechanical systems (MEMS) are fabricated using similar processes and will benefit from further reductions in minimum feature size over time. Micro/nanoelectronics and micro/nanoelectromechanical systems will evolve over the next decade to provide ever-higher levels of functional density per unit area.

Small spacecraft, particularly picosatellites and CubeSats, require mm-to-cm scale sensors for attitude determination. Commercial CMOS technology provides mm-to-cm scale image sensors that can function as sun and star sensors while MEMS technology offers mm-to-cm scale magnetic and inertial sensors. Custom CMOS/MEMS technology enables mm-scale sun and horizon sensors suitable for picosatellites and even smaller spacecraft. Several examples of millimeter and centimeter-scale sun sensors are given.

1.0 PICOSATELLITE HISTORY

Figure 1 shows the yearly on-orbit deployment rates of picosatellites; satellites with a mass between 0.1 and 1-kg. The 1960's witnessed only 3 picosatellite deployments (2 active, 1 passive), the 1970's provided only 4 (all passive), the 1980's had none, and the 1990's saw only 3 (all passive). Fortunately, average launch rates picked up significantly starting in the year 2000.

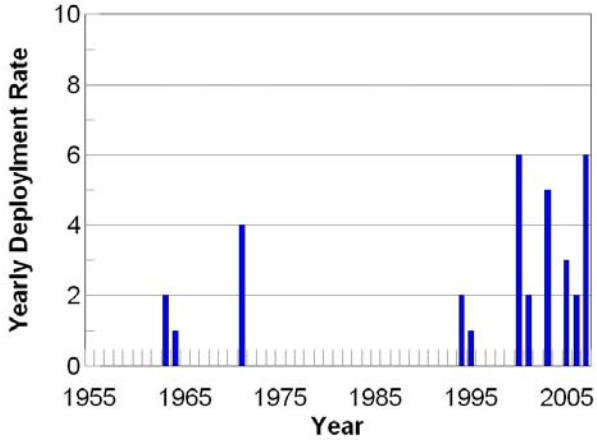

Figure 1. Yearly on-orbit deployment rate for picosatellites as a function of calendar year.

The first picosatellites were launched in May 1963 as part of the USAF Environmental Research Satellite (ERS) series. ERS-5 and ERS-6 were 0.7-kg mass, tetrahedral, solar-powered, active spacecraft with 13-cm long side lengths, and were also known as Tetrahedral Research Satellites (TRS) TRS-2 and TRS-3. ERS spacecraft were used as technology test beds for spacecraft systems and components at medium Earth altitudes (greater than 1,500-km apogee). Due to their high perigees, ERS spacecraft were in sunlight most of the time and did not need batteries or battery charge regulators. The third deployed picosatellite, a passive 0.98-kg mass sphere called Calsphere-1, was launched in October 1964 along with a passive 9.8-kg mass sphere (Calsphere-2). Both spacecraft were 14" (35.6-cm) diameter, polished aluminum hollow spheres that were simultaneously injected into almost identical, 1000-km altitude polar orbits.[1,2] These Calsphere satellites were used as radar targets and as atmospheric density monitors; the latter application used orbital tracking data over time to determine satellite drag levels and hence atmospheric density vs. altitude.

Three 26-cm diameter, 730-gram mass hollow aluminum spheres (Calsphere-3, Calsphere-4 and Calsphere-5) were launched in February 1971 to study the effect of surface composition on atmospheric drag.[3]

The final picosatellite of the 1970's was a 2.13-meter diameter, 0.8-kg mass Mylar balloon that was deployed in August 1971.[4]

A series of passive small satellites were ejected from U.S. Space Shuttles in 1994 and 1995 as part of the Orbital Debris Radar Calibration Sphere (ODERACS) experiment. ODERACS 1, flown on STS-60 in February 1994, deployed six spheres: two 15-cm diameter, 5-kg aluminum spheres, two 10-cm diameter, 1.49-kg mass aluminum spheres, and two 5-cm diameter, 0.53-kg stainless steel spheres.[5,6] ODERACS 2, flown on STS-63 in February 1995, deployed a 15-cm, 5.00-kg mass aluminum sphere, a 10-cm, 1.49-kg mass aluminum sphere, a 5-cm diameter, 0.53-kg stainless steel sphere, two 13.3-cm long by 0.102-cm diameter dipoles with ~1.5 gram mass, and one 4.42-cm long by 0.102-cm diameter dipole with ~0.5 gram mass. In total, ODERACS deployed three passive picosatellites. ODERACS showed that at least 10-cm diameter objects could be tracked, and that even an electronically "dead" nano/picosatellite could be used to provide atmospheric density measurements by monitoring its altitude as a function of time.[7]

The picosatellite revolution occurred on January 27, 2000, when an Orbital Sciences Minotaur rocket put JAWSAT into orbit. JAWSAT released the 22-kg Optical Calibration Sphere Experiment (OCSE; a 3.5-m diameter balloon), the 52-kg Falconsat-1 from the U.S. Air Force Academy, the 5-kg ASUsat-1, and the 25-kg mass OPAL. OPAL subsequently ejected three picosatellites from Santa Clara University (the 0.2-kg Jak, the 0.5-kg Thelma, and the 0.5-kg Louise), a 0.23-kg amateur radio picosatellite called Stensat, and two 0.3-kg DARPA/Aerospace Corp. "PicoSats."[8] Two more DARPA/Aerospace PicoSats rode into orbit on the second Minotaur launch on July 19, 2000 inside the 120-kg MightySat-II.1 spacecraft built by the Air Force Research Laboratories, and were ejected in August 2001. More picosatellites had been orbited in the year 2000 than in any previous single year, and more active picosatellites had been deployed than ever before (6 in 2000 vs. 2 from 1957 through 1999).

The Aerospace Corporation designed and built the PicoSats for DARPA along with Rockwell Science Center (RSC). Rockwell had developed MEMS radio frequency switches under contract to DARPA, and they designed and built the 915-MHz communications boards for the spacecraft. These transceivers demonstrated a low-power (65-mW) communications-hopping protocol originally developed for unattended ground sensors. Two PicoSats were therefore attached by a 30-m long tether and ejected together as a pair. Figure 2 shows a photograph of a PicoSat with one side panel replaced by a partially-transparent sheet in order to show the interior. The electronics reside on three 2.2" (5.6-cm) square circuit boards and the spacecraft was powered by lithium thionyl chloride primary batteries with a total capacity of 10 W-hr. Two patch antennas, one on each 3" x 4" surface, were used to provide an almost hemispherical antenna pattern. Note that no attitude control or propulsion was required for this mission. These picosatellites were, and still are, the lightest active satellites ever deployed on-orbit.

Figure 2. Photograph of The Aerospace Corporation's 1' x 3" x 4" (2.5 x 7.5 x 10-cm) PicoSat.

The success of OPAL eventually led to the establishment of the CubeSat program initiated by Stanford and the California Polytechnic State University – San Luis Obispo that will probably put hundreds of nano/picosatellites into orbit over the next decade. All of the picosatellites launched since 2003 (see Fig. 1) have been single CubeSats. Although they are not listed in Table 1 since the current calendar year hasn't ended, an additional 3 single 10-cm cube CubeSats (AAUSAT-II, COMPASS-1 and SEEDS2) were launched on April 28, 2008. Note that the average launch rate of CubeSats has been 3.2 per year over the last 5 years.

So far, The Aerospace Corporation has fabricated two CubeSats. AeroCube-1 was destroyed by a launcher failure in July 2006, but AeroCube-2 was successfully launched in April 2007. We are currently working on AeroCube-3.

2.0 COTS MICRO/NANOTECHNOLOGIES

Most picosatellites launched between 1963 and 1999 were passive, but that changed in the year 2000. Further increases in the functional density of commercial off the shelf (COTS) microelectronics, plus improvements in solar cell efficiency, the energy storage density of secondary batteries, and miniaturized optical, magnetic, and inertial sensors now made intelligent and capable picosatellites possible. Nanosatellite and even some microsatellite capabilities could be put into the smaller, lighter picosatellites.

2.1 Microelectronics

In 1965, Gordon Moore noticed that the complexity of integrated circuits, for lowest cost per component, doubled roughly every year due to advancements in technology.[9] That trend, now known as Moore's Law, has held for central processing units (CPU) and dynamic random access memory (DRAM) chips for the last 42 years. The doubling of microprocessor performance every 24-to-30 months was driven by the ability to produce ever-smaller and faster transistors. The Intel 4004 microprocessor, introduced in 1971, had 3,200 transistors and was fabricated with 10-micron minimum feature size (MFS). All satellites designed before 1971 did not use microprocessors; they used multiple functional logic circuits to perform command and control functions. After 1971, an entire board full of 2-to-4 cm long ceramic integrated circuit packages could be replaced by a single, roughly 2-cm long package.

The Intel 80286 microprocessor, introduced in 1982, was a 1 million instruction per second (MIPS) processor with 134,000 transistors fabricated using 1.5-μm MFS on a 69 mm^2 silicon die. This processor was used in the IBM AT series of personal computers. In the year 2000, Intel introduced the Pentium IV with 42 million transistors fabricated using a 0.18-micron MFS, resulting in transistor area less than a square micron.[10] In 2008, Intel will release the Tukwilla microprocessor with 2-billion transistors, fabricated using a 65-nm MFS process.[11] A team of international scientists and engineers monitor historical trends, track advancements in fabrication technologies, and predict future capabilities and technology limitations in semiconductor fabrication. They produce The International Technology Roadmap for Semiconductors (ITRS) that gets updated every two years. Their current prediction includes 45-nm MFS by the year 2010, 25-nm MFS by 2015, and 14-nm MFS by the year 2020.[12] Significant challenges exist in meeting these goals, but Moore's Law should continue to operate for at least another decade.

How much silicon area is required for a ~ 1-MIPS (million instructions per second) microprocessor suitable for basic small satellite command and control functions? Figure 3 shows the past, present, and future size of this processor based on historical and ITRS predictions of minimum feature size. Space-qualified processors will be somewhat larger due to extra integrated structures (e.g., transistor guard bands and fault detection and correction circuitry), but 80286-class processors can still be extremely small. By the year 2016, this class of processor could be fabricated on a silicon die with a side length about twice that of a human hair. Figure 3 also shows the DRAM die size required to hold 1 million words (8 bits of data plus 4 extra bits for error detection and correction) of memory. Today, the processor and memory could fit on a 1-mm^2 die with room to spare. The MicroChip PIC10F222 is an example of a current-generation ultra-small microprocessor available to the masses. It comes in an 8-lead DFN package (2-mm x 3-mm x 0.9-mm) and includes two 8-bit analog input channels.[13] Figure 4 shows a photograph of this Lilliputian processor.

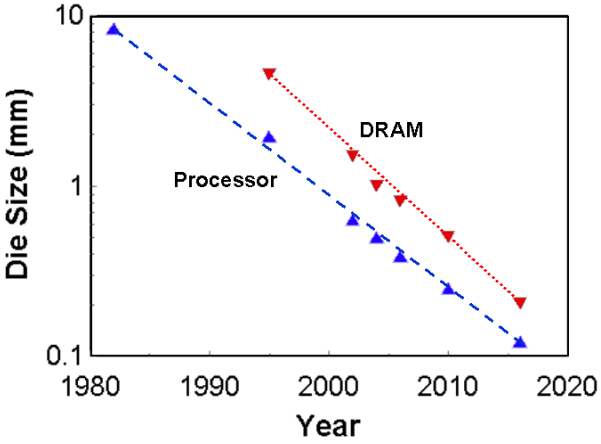

Figure 3. Die size for an Intel 80286-class micro-processor and a 1 Mbyte DRAM as a function of time.

The continuing reduction in MFS has also enabled an increase in processor efficiency based on smaller transistors with reduced operating voltage. Low-power microprocessors and microcontrollers are now available with processing performance on the order of 3000-MIPS/W. The Microchip PIC10F222 requires less than 350-μW (175-μA at 2-Volts) when operating at 4-MHz (1-MIPS). While the computational power efficiency is high at 2800-MIPS/W, this microcontroller has only

Figure 4. Photograph of a MicroChip PIC10F222 microprocessor on a U.S. dime. (A U.S. dime is ~18-mm in diameter)

768 bytes of program memory. It's suitable for simple tasks like timing functions and converting analog sensor outputs into digital outputs. The more capable Microchip PIC18F1320 microcontroller, with 7 analog inputs, 16 input/output lines, and 16 kilobytes of program memory, requires about 300-μW (150-μA at 2-Volts) when operating at 1-MHz (0.25-MIPS).[14] This results in a performance rating of 833-MIPS/W; a 1-MIPS command and control computer would consume about 1.2-mW. We use this processor, along with other MicroChip PIC processors in our AeroCubes and other small satellite projects. Other examples of ultra low power processors include NEC's VR4131 microprocessor (340-MIPS @ 220-mW; 1545-MIPS/W) and the Atmel AT91R40807 processor used on the CanX-1 (University of Toronto) CubeSat (~1.4-mW/MHz and 36-MIPS @ 40-MHz; 643-MIPS/W).[15,16,17,18] Current-generation low-power processors operate at 1 to 2-Volts, but ultimate operating voltages based on CMOS technology could be between 0.2 and 0.3-Volts for significantly reduced power consumption. Reference 19 gives an excellent review of CMOS scaling and voltage limitations.

2.2 CMOS Image Sensors:

One of the benefits of an aggressive semiconductor fabrication industry is the development of related products that leverage existing fabrication infrastructure. Active pixel sensors were invented in the early 1990's at NASA-JPL to circumvent multiple problems with Charge Coupled Devices (CCDs).[20, 21] These CMOS-fabricated devices use transistors co-located with 2 to 8-micron square p-n photodiode light sensors to amplify the signal and route it to an appropriate addressing line for readout. Inexpensive mass-production of active pixel image sensors for digital cameras, web cameras, wireless telephones, etc., is a byproduct of CMOS compatibility. Larger pixels (~7-microns square) are typically offered on VGA resolution cameras (640 x 480 pixels) while ~2-micron square pixels are offered on 5-megapixel imagers.

Table 1 shows array size, pixel size, and operating power for some current CMOS image sensors. These are all based on active pixel technology. 4 years ago, this table had resolutions ranging from 288 by 362 pixels to 1032 by 1288 pixels with pixel sizes between 5.2 and 7.8 microns on a side. Further reductions in transistor size during the last 4 years have enabled 2-micron square pixels with enough area for the photodiode plus addressing transistors. To first order, power is a function of frame rate so the power values can be scaled down if slower image acquisition is desired. At a frame rate of 10 images per second, the power consumption for this group varies from 13-mW (OmiVision OV7141) for a 640 by 480 array (0.3 megapixels) to 270-mW (Micron MT9P031) for a 2592 by 1944 array (5-megapixels). The 28-pin CLCC, 48-pin CLCC, and 48-pin iLCC packages in Table 7 are square with side dimensions of 11.2-mm, 14.2-mm, and 14.2-mm, respectively. Imagers like the STMicroelectronics VS6727 2-megapixel single-chip camera module include hardware image compression. Figure 5 shows a photograph of a COTS camera board that includes JPEG (Joint Photographic Experts Group) compression.[22] This 2.0 x 2.8-cm board has a mass of 10-grams, a maximum power usage of 200-mW, and uses a ¼" (6.4-mm) 640 x 480 color CMOS imager with a lens. We have successfully used this imager on our MEMS Picosatellite Inspector and AeroCubes.[23]

Table 1. Characteristics of representative color CMOS imagers. Data from references 24, 25, 26, 27, 28, 29, 30, 31.

Device	Array Size	Pixel Size (μm)	Package	Power (mW)
OmniVision OV7141	640 x 480	5.6 x 5.6	28-pin CLCC	40 @ 30 frame/s
OmniVision OV3630	2048 x 1536	2.2 x 2.2	6.1 x 6.3-mm	110 @ 15 frame/s
Micron MT9V011	640 x 480	5.6 x 5.6	28-pin LCC	70 @ 30 frame/s
Micron MT9D131	1600 x 1200	2.8 x 2.8	48-pin CLCC	348 @ 15 frame/s
Micron MT9P031	2592 x 1944	2.2 x 2.2	48-pin iLCC	381 @ 14 frame/s
STMicroelectronics VS6724	1600 x 1200	2.2 x 2.2	7.8-mm square	300 @ 30 frame/s
Kodak KAC-9628	648 x 488	7.5 x 7.5	48-pin CLCC	168 @ 30 frame/s
Kodak KAC-01301	1284 x 1028	2.7 x 2.7	48-pin CLCC	100 @ 16 frame/s

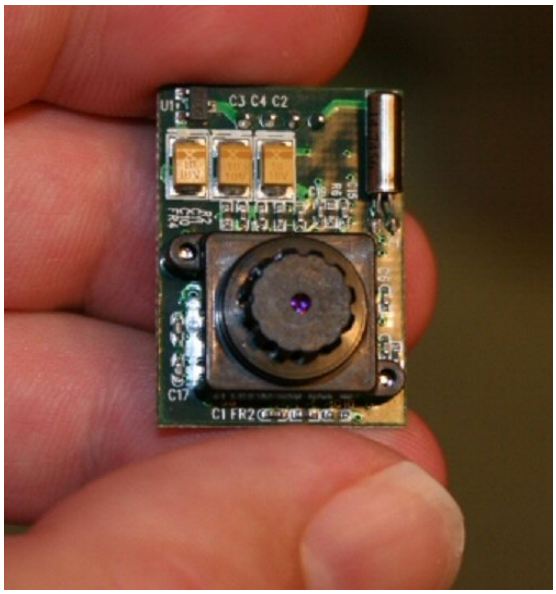

Figure 5. Photograph of the C328 camera board with lens.

CMOS image sensors are typically sensitive to wavelengths between 400-and-1100 nm. Visible light spans 400-to-700 nm, so a ~400-nm band of invisible near-infrared (near-IR) radiation can be sensed by these devices. This can be useful for Earth observation since plants are very reflective in the near-IR. Figure 6 shows images of the same scene taken using the camera shown in Fig. 5 with (right; near-IR image) and without (left; visible light) a near-IR bandpass filter. The near-IR filter allows wavelengths between 700-nm and 1200-nm to pass through, but blocks visible light. Note that the trees and grass are almost white in the near-IR image.

CMOS image sensors can also be used in star trackers. Star trackers on spacecraft take images of star fields that are subsequently processed by on-board computers to calculate pointing direction (two orthogonal reference angles) and rotation (third angle) about the direction vector. The process includes measurement of angles between visible stars and comparison of those angle sets against a stellar database. Use of stars down to magnitude 4 provides a reasonable number of visible stars in any frame if the frame field of view is at least 40^{o}.[32] If a 4-Megapixel or greater imaging array is used as the detector, 3-axis angular orientation can be determined to about 0.02^{o}, or 0.35-milliradians; this is very good pointing accuracy for a picosatellite.

How large does the imaging optic have to be in order to see 4th magnitude stars? Figure 7 shows a 2-second long photograph of the constellation Orion taken near sea level using a commercial Canon EOS20D single lens reflex camera at an f-stop of 3.5 with a 18-mm focal length lens. While not obvious in Figure 7, stars down to magnitude 3.4 are seen using this effective aperture of 5.1-mm. Based on this image, a lens with a 1" diameter clear aperture would gather enough light in 0.1 seconds to see stars down to 4th magnitude. The entire star tracker with this size optic would fit on a CubeSat with room to spare.

Figure 6. Two CMOS camera images of the same scene with (right) and without (left) a near-IR bandpass filter.

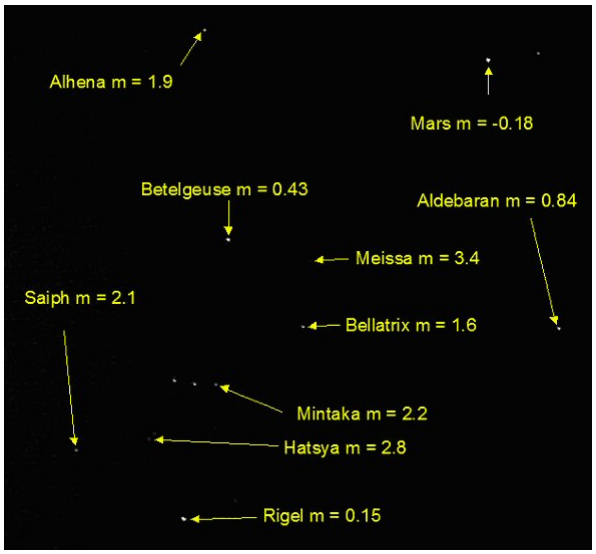

Figure 7. The constellation Orion and neighboring stars taken by a terrestrial digital camera using a 2-second exposure and an 18-mm focal length, f-3.5 lens.

2.3 Magnetic Field Sensors:

In LEO, crude (about a degree) orientation about two axes can be determined by measuring the local magnetic field vector. Spacecraft in low Earth orbit (LEO) have typically used flux-gate magnetometers to measure local magnetic field strength and direction, but magnetoresistive sensors have now become suitable for determining attitude with respect to the Earth's magnetic field. An example of a microfluxgate sensor based on a modified CMOS process is given in reference 33. This 0.8 x 1.5 mm sensor uses a ferromagnetic layer deposited on top of the die passivation layers and has a linear response to magnetic fields below 50 μT with a maximum sensitivity of 2.7 V/T. MEMS-based magnetic field sensors have also been fabricated.[34,35] Magnetic field sensors utilizing the giant magnetoresistive field effect (resistance is a function of applied magnetic field) are commercially-available from Honeywell.[36] A number of CubeSats have used the Honeywell HMC2003 sensor that provides analog output voltages that can be read by analog to digital converters embedded in many microprocessors.[37] This 2.7-cm x 2.00-cm x 1.2-cm hybrid module contains sensors and signal amplifiers. It uses 120-mW of power at 6 Volts and can resolve 40 μG; this corresponds to 0.02% of the ambient magnetic field at the equator at an altitude of 700-km.

2.4 MEMS for Inertial Sensing:

Accelerometers can be used to measure instantaneous accelerations due to thruster operation, air drag, solar pressure, etc. MEMS accelerometers are used in automobiles for crash detection, in wireless 3D computer mice, in transport shock monitors, and in various tilt/leveling applications (e.g., an electronic level). MEMS accelerometers are particularly convenient for small satellites due to their small size and low power requirements. Many manufacturers exist and the maximum sensing range varies from +/- 1.5 g's to +/- 100 g's.

Inexpensive commercial accelerometers like the Analog Devices ADXL103 are chip-size devices (5 x 5 x 2-mm) that can measure spacecraft accelerations down to the 0.1 milli-g level using less than 5-mW of power. This would provide 1-mN resolution on a 1-kg mass CubeSat; adequate for cold gas and chemical thrusters in the 10-mN thrust range and higher. More expensive MEMS devices such as the Colibrys Si-Flex SF-1500S is a small board-sized device (24.4 x 24.4 x 16.6-mm) that can measure accelerations down to the 0.3 micro-g level using ~70-mW of power. This would provide 3-micronewton resolution for monitoring high specific impulse thrusters on a CubeSat. A 1-W, 3000 s specific impulse ion engine, for example would produce 34-microNewtons of thrust at 50% thrust efficiency.

Rate gyros are used on small spacecraft to monitor angular rate changes due to magnetorquing, momentum wheel operation, or thruster operation. MEMS rate gyros have been developed for automobile (skid control), movie/video (image stabilization), and computer (wireless mouse) applications and are typically based on tuning fork structures where Coriolis accelerations create out-of-plane motion. Commercial MEMS gyros are not suitable for inertial navigation beyond a few minutes, but they are suitable for monitoring spacecraft rotation rates significantly faster than orbit rates in LEO (360^o in ~90 minutes; 0.067^o/s). For example, the Analog Devices ADIS16250 comes in a 11.1-mm x 11.0-mm x 5.3-mm package, consumes only 40-mW of power, and has a noise density of $0.05^o/s/Hz^{1/2}$.[38] It can be used to provide a 1^o pointing accuracy over a 2-minute period.

3.0 CUSTOM MICRO/NANOTECHNOLOGIES

One can design custom application-specific integrated circuits for specific applications and have them fabricated by a prototyping service such as the Metal Oxide Semiconductor Implementation Service

(MOSIS).[39] MOSIS aggregates die designs from multiple customers into a single mask set for fabrication by a particular process, thus allowing individual customers to share setup and fabrication costs. MOSIS currently offers a wide variety of CMOS processes with minimum feature sizes ranging from 65-nm to 1.5-microns. The MOSIS accepts designs from commercial firms, government agencies, and research and educational institutions around the world. A single mask set for a CMOS integrated circuit can cost $50,000 and up, depending on the minimum line feature size and number of layers required. A 2-mm square "tiny chip" fabricated using a 1.5-micron CMOS process costs about $1100 for 5 copies. This low-cost fabrication service is ideal for students and researchers who need only a few copies of a given design or need to verify their designs before they enter mass-production.

Chip designers typically combine functional blocks like logic gates, operational amplifiers, analog multiplexers, etc. from CMOS libraries to build the desired functionality into a single die. Tanner Tools, for example, sells several mixed-signal (analog and digital) circuit design kits for the 1.5 to 0.18-micron MFS range.[40] More experienced designers have the option of designing individual transistors and their interconnects to create unique circuits and photodetector arrays of arbitrary shape. I have used the custom CMOS approach using CMOS circuit libraries with custom-designed detectors to build 2.2-mm square active pixel detectors for sun sensors and thermopile detector arrays for Earth sensors.[41,42]

This custom-designed CMOS option also enables increased radiation tolerance through proper transistor and circuit design. One commercially-available 0.25-μm process started with an apparent total dose limit of greater than 100 kilorads that was increased to greater than 500 kilorads with the addition of guard bands, etc.[43]

4.0 SUN SENSORS FOR PICOSATELLITES

The simplest optical attitude sensor is the sun sensor. Many commercial sun sensors are too large for CubeSats, and cm-scale or even mm-scale designs are desirable for picosatellites in general. The Technical University of Denmark has already demonstrated custom sun sensors for use on the DTU CubeSat.[44] The photodetectors are fabricated on a silicon-on-insulator die which is bonded to a Pyrex die with a patterned aluminum coating; two single-axis sensors are fabricated on a single ~ 6-mm x 7-mm die. The sensor has a +/- 70^o field-of-view and a theoretical resolution of 0.07^o. This section will outline three approaches taken at The Aerospace Corporation to create two-axis sun sensors.

4.1 Custom CMOS Sensors

An example of one of our early prototype CMOS Sun sensors "on a chip" is shown in Fig. 8.[41] This 2.2-mm square CMOS die was fabricated using a 1.5-μm process and includes a 10 x 10 array of active pixel sensors with 82.5-μm pitch. Each pixel includes a 46 x 46-μm detector and three transistors for row and column selection plus reset. The light rectangles around the periphery of the circuit are the bond pads that get wire-bonded to a chip carrier. These pads and their driver circuits were designed using a Tanner Tools CMOS library while the photodetectors and addressing transistors were custom-designed. This prototype detector chip was designed for a resolution of 4^o and a field-of-view of 90^o when coupled to 2-mm thick fused silica block with appropriate surface coatings to create a pinhole lens; the fused silica acted as a radiation shield.

The chip shown in Fig. 8 was used as a learning tool and was not intended for actual flight. One of the drawbacks of using the particular 1.5-microm MOSIS process was the ~8-week interval between process runs and the 10 to 12-week fabrication time. It would take 6 months to submit a design, get the processed dice, test the dice, make modifications, submit an improved design, and get the improved dice for testing. Fortunately, processes with smaller MFS occur more frequently, thus reducing cycle time. This approach, however, can cost 3 to 10 times more due to increased processing costs at lower minimum feature sizes.

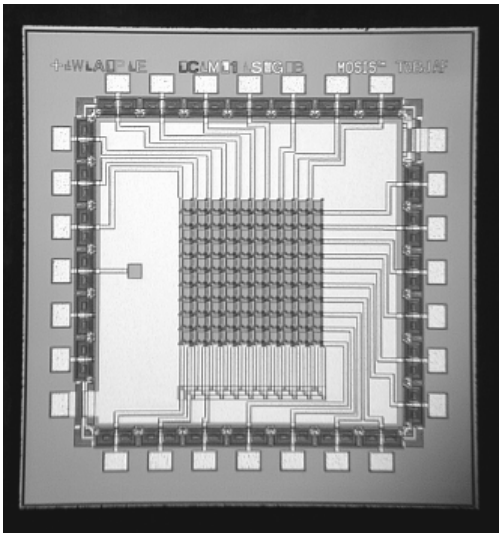

Figure 8. A two-dimensional active pixel sensor array fabricated using a 1.5-micron CMOS process, suitable for use as a Sun sensor in small spacecraft.

4.2 COTS Analog Position Sensors

I designed a two-axis sun sensor for upcoming AeroCube and small satellite flights that uses a commercially-available position sensitive detector (PSD) coupled to a pinhole as shown in Figure 9. A small aperture allows directed sunlight to impinge on a PSD. The PSD has 4 electrodes located near the outer edges of the square detector, and the photocurrents collected by each electrode uniquely specify an X-Y location on the PSD that corresponds to the centroid of illumination. This ultimately yields the angular position of the sun with respect to the surface normal of the sun sensor. This approach has been used on the AMSAT Phase 3D satellite and the upcoming AMSAT Eagle and KiwiSAT satellites.[45,46] The PSDs for these missions were ~ 1-cm square (typically a Hamamatsu S5991-01). Our sun sensors use a smaller Hamamatsu S7848 PSD with a 2-mm x 2-mm active area.[47] The detector chip, including electrical contacts, is 7-mm x 5-mm x 1.8-mm in size.

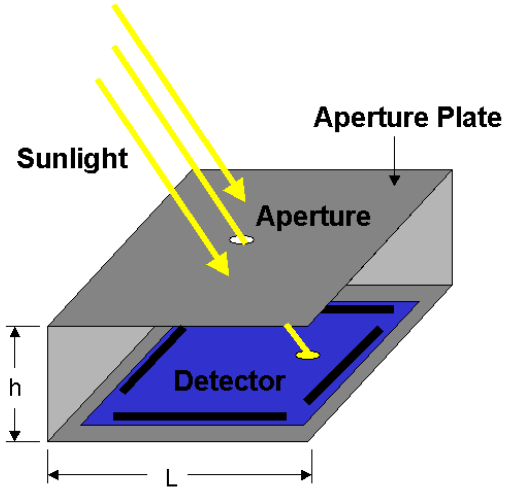

Figure 9. Schematic diagram of a basic 2-axis sun sensor using a position-sensitive detector.

In typical operation, the PSD is operated in reverse-bias mode where the cathode is held at +0.1 to +20-Volts and the photocurrents are measured at each anode. The inter-electrode resistance is ~100-kOhms, the photosensitivity at 800-nm is 0.58-A/W, the saturation photocurrent is ~100-microamperes, and the position detection error is +/- 20 microns within 0.75-mm from the center of the detector.

The basic mechanical design for moderate radiation environments is shown in Figure 10. The sensor is encased in a transparent plastic, and the detector surface is 0.5-mm below the top surface of the chip. An aperture plate (pinhole) is bonded directly to the top surface, and the PSD chip is soldered to a circuit board that contains the analog and digital circuits. We mount the detector board inside the spacecraft to provide radiation shielding and a stable thermal environment. A BK-7 glass window provides optical access to the outside world, some radiation shielding, and filtering of sunlight to within a 350-nm to 3000-nm wavelength range. The latter function blocks ultraviolet light which can damage the clear plastic in the PSD chip.

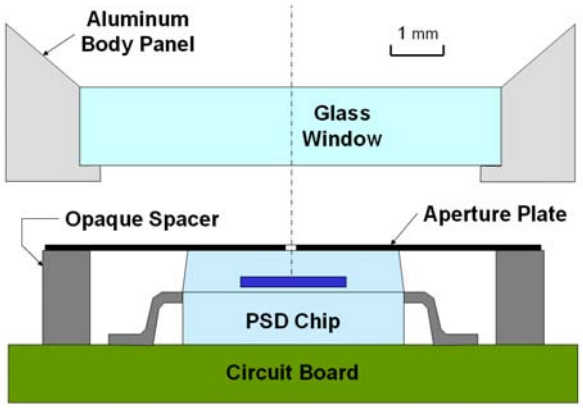

Figure 10. Schematic cross section of the main sun sensor components mounted inside a spacecraft with aluminum outer walls.

We use a 200-micron diameter aperture that lets 40-microwatts of filtered in-space sunlight impact the detector when the sun is normal to the sensor. The maximum current output is 25-microamperes. Four transimpedance amplifiers are used to convert the 0 to 25-microampere current outputs from the individual electrodes to 0 to 5-Volt outputs that are read by a MicroChip 18F1320 microcontroller. The micro-controller performs analog to digital conversions, calculates the X and Y-axis positions of the centroid using integer math, and broadcasts the results serially on an SPI bus.

Measured X and Y-axis position data for sunlight hitting the assembled detector as a function of incidence angle is shown in Fig. 11. These data were taken under in-space AM0 (Atmospheric Mass Zero; raw sunlight in space) conditions provided by a SpectraLabs X-25 solar simulator. In this case, the aperture was well centered and the X and Y positions are fairly linear over a +/- 40° range. The traces curve towards the vertical axis at incidence angles greater than 30° due to refraction in the 0.5-mm thick plastic between the pinholes and the silicon detector surface. Angular measurements had an accuracy of +/- 0.5° and the position measurements had an accuracy of +/- 0.02-mm based on the detector specifications. Raw solar incidence angle accuracy is presently +/- 2° over a +/- 30° incidence range due to

position sensor errors and refraction. This will be further reduced over a wider +/- 50° incidence range through sensor calibration in the solar simulator. The 2-axis sun sensor consumes less than 10-mW.

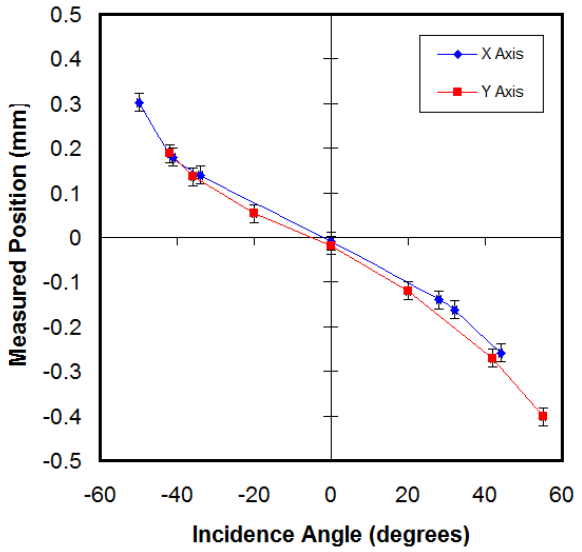

Figure 11. Measured X and Y-axis outputs for the sun sensor as a function of X and Y angles of incidence.

4.3 CMOS Camera Sensors

Inexpensive, low power image sensors enable a wide variety of attitude sensing and payload sensor applications. A simple yet sophisticated Sun sensor could integrate a low-resolution CMOS image sensor with a wide angle lens or pinhole. VGA imagers with about 500 pixels per line provide about 0.2° of angular resolution per pixel with a moderate 100° field-of-view. The Sun has an angular diameter of about 0.5°, so it will light up from none to four pixels along any row or column. Mapping the two-dimensional intensity distribution near the Sun's image and applying fitting algorithms will enable sub-pixel determination of the Sun's centroid along two orthogonal axes to at least 0.3 pixels. In this case, one uses a complex, but fairly inexpensive commercial imager with image processing algorithms running on a low power microprocessor. A dedicated microcontroller would identify the Sun's image, reject image clutter from the Earth and Moon, correct for image plane distortions, and calculate the position of the Sun's centroid within a tenth of a degree (0.2°/pixel x 0.3 pixel resolution). We are currently investigating this approach using CMOS image sensors similar to the one shown in Fig. 5 for future applications.

5.0 CONCLUSIONS

Up until the year 2000, only a two active picosatellites had been put into orbit. For the first 40 years of the Space Age, it was difficult to integrate high levels of functionality into the picosatellite 0.1 to 1-kg mass range and most picosatellites were passive balloons or spheres used for atmospheric density measurements and radar calibration. Today, continuing advancements in micro/nanoelectronics have provided highly-capable, low-power microprocessors and microcontrollers that operate at microwatt to milliwatt power levels. Gigabytes of memory can now fit on less than a square centimeter. Picosatellites can have multiple, distributed processors and enough memory storage to support continuous downloading of data for an entire day at data rates of a megabit/s.

The current challenge is to incorporate attitude determination and control systems into picosatellites for Earth imaging sensors, sun-tracking solar arrays that can provide more than a Watt of orbit-average power, and medium gain antennas to improve communications link budgets for high-speed data transfer. Centimeter-scale magnetic sensors, MEMS inertial sensors, and visible image sensors are commercially available, but low-power mm-to-cm scale sun, Earth and star sensors are still needed. Custom CMOS/MEMS technology enables mm-scale sun and horizon sensors suitable for picosatellites and even smaller spacecraft. Active femtosatellites (mass between 0.01 and 0.1-kg) with attitude determination and control should appear within a few years. For those engineers with less time, cm-scale sun sensors can be built using commercial off the shelf position-sensitive detectors or CMOS imagers.

Note: All trademarks, service marks, and trade names are the property of their respective owners.

Acknowledgements
I gratefully acknowledge The Aerospace Corporation's Independent Research and Development program and its former Corporate Research Initiative in MEMS and Microtechnology for funding the development of CMOS-based sensors. I also want to thank The Aerospace Institute for sponsoring my chapter "Small and Really Small Satellites: The Nanosat Concept" in the upcoming AIAA/Aerospace Institute book *Small Satellites: Past, Present and Future* to be published in Nov/Dec 2008. The historical sections of this paper were extracted from that chapter (My chapter, one of 23, needed a reduction in length!). Finally, I want to thank David Hinkley, Daniel Rumsey, Petras Karuza, James Swenson, and Simon Liu of The Aerospace Corporation for their assistance in fabricating and testing the PSD-based sun sensor.

References

1. Zirm, R.R., Brescia, R.E., and R.S. Rovinski, *The Dual Calsphere Experiment*, Interim Report, Naval Research Laboratoratories, Washington, D.C., July 1965.

2. Zirm, R., Easton, R., Kleczek, C., and R. Rovinski, "NRL Calibration Spheres," Proc. of the IEEE, pp. 396-397, Vol. 54, #3, Mar. 1966.

3. Zirm, R.R., "The Triple Calibration Sphere (CALSPHERE) Experiment," Proc. of the IEEE, pp. 1725-1726, Vol. 59, #12, Dec. 1971.

4. National Aeronautics and Space Administration, "Mylar Balloon" page of the National Space Science Data Center Catalog, URL: http://nssdc.gsfc.nasa.gov/nmc/masterCatalog.do?sc=1971-067F , 2007.

5. NASA Orbital Debris Program Office, The Orbital Debris Radar Calibrations Spheres web page, URL: http://www.orbitaldebris.jsc.nasa.gov/measure/oderacs.html , 2007.

6. Cress, G.H., Potter, A.E., Setticeri, T.J., Sherrill, G.P., Stansbery, E.G., Talent, D.L., 1996. Radar and optical ground measurement, Final report, Orbital debris calibration spheres. NASA Report JSC-27241, NASA Johnson Space Center, Houston.

7. Tan, A. and Badhwar, G.D., "Detecting the Dynamical State of the Atmosphere from the Orbital Decay of the ODERACS Spheres," Journal of Atmospheric and Solar-Terrestrial Physics, Vol. 59, #4, pp.431-437, March, 1997.

8. Cutler, James, and Hutchins, Greg, "OPAL: Smaller, Simpler, and Just Plain Luckier," Proc. Of the 14th annual AIAA/USU Conference on Small Satellites, Ogden, Utah, Aug., 2000.

9. Moore, Gordon E., "Cramming More Components Onto Integrated Circuits," *Electronics*, pp. 114-117, **38** #8, April 1965.

10. Intel "Moore's Law" page, available online at http://www.intel.com/research/silicon/mooreslaw.htm, 2002.

11. Intel, "World's First 2 Billion Transistor Microprocessor," Intel Corporation, Santa Clara, CA, URL: http://www.intel.com/technology/architecture-silicon/2billion.htm?iid=tech_arch+body_2b , 2008.

12. International Technology Roadmap for Semiconductors, "Executive Summary, 2007 Edition," URL: http://www.itrs.net/Links/2007ITRS/ExecSum2007.pdf

13. Microchip, PIC10F220/222 datasheet, Microchip Technology Inc., Chandler, Arizona, URL: http://ww1.microchip.com/downloads/en/DeviceDoc/PIC10F220222%20Data%20Sheet_41270E.pdf , 2008.

14. Microchip, PIC18F1220 datasheet, Microchip Technology Inc., Chandler, Arizona, URL: http://www.microchip.com/1010/pline/picmicro/category/embctrl/8kbytes/devices/18f1220/index.htm

15. Motorola Inc. presentation "M*CORE Review," Motorola Semiconductor Products Sector, available on-line at: http://e-www.motorola.com/brdata/PDFDB/docs/MCORECUST.pdf , 2007.

16. NEC Corp. VR 4131 product brochure, available on-line at: http://www.necelam.com/docs/files/U15396EU3V0PB00.pdf , 2007.

17. Atmel Corp. datasheet, "AT91R40807 Electrical Characteristics," available on-line at: http://www.atmel.com/dyn/resources/prod_documents/DOC1367.PDF , 2007.

18. Wells, G. James, Stras, Luke, and Jeans, Tiger, "Canada's Smallest Satellite: The Canadian Advanced Nanospace eXperiment (CanX-1)," Proc. 16th AIAA/USU Conference on Small Satellites, 2002.

19. Philip, Hon-Sum et al., "Nanoscale CMOS," *Proceedings of the IEEE*, pp.537-570, **87** #4, April 1999.

20. Fossum, Eric R., "Active Pixel Sensors: Are CCDs Dinosaurs?," Proc. Of the SPIE, Vol. 1900, Charge-Coupled Devices and Solid State Optical Sensors III, Morley M. Blouke, Editor, pp.1-14, July 1993.

21. Fossum, Eric R., "CMOS Image Sensors: Electronic Camera-on-a-Chip," IEEE IEDM Tech. Dig. Pp. 17-25, Dec. 1995.

22. Joint Photographic Expert Group home page, URL: http://www.jpeg.org/index.html , 2007.

23. Hinkley, David, "A Novel Cold Gas Propulsion System for Nanosatellites and Picosatellites," 22nd Annual AIAA/USU Conf. On Small satellites, paper SSC08-VII-7, 2008.

24. OmniVision product brief, "OV7640 Color CMOS VGA CameraChip," OmniVision, Sunnyvale, CA, URL: http://www.ovt.com/data/parts/pdf/OV7640_PB%20(2.1).pdf , 2008.

25. Micron Technologies technical brief, "MT9V011 data sheet," Micron Technologies, Boise, ID, URL: http://download.micron.com/pdf/datasheets/imaging/MT9D011_MI2010_E.pdf , 2008.

26. Micron Technologies technical brief, "MT9D131 data sheet," Micron Technologies, Boise, ID, URLt: http://download.micron.com/pdf/product_brief/MT9D131_PB.pdf , 2007.

27. Micron Technologies technical brief, "MT9P031 data sheet," Micron Technologies, Boise, ID, URL: http://download.micron.com/pdf/product_brief/MT9P031_5100_PB.pdf , 2007.

28. OmniVision product brief, "OV3630 3.2 MPixel," OmniVision, Sunnyvale, CA, URL: http://www.ovt.com/data/parts/pdf/Brief3630V2.1.pdf , 2007.

29. STMicroelectronics datasheet, "VS6724 2 Megapixel Single-Chip Camera Module," STMicroelectronics, Geneva, Switzerland, URL: http://www.st.com/stonline/products/literature/ds/13399/vs6724.pdf , 2007.

30. Kodak data sheet, "KAC-9628," Eastman Kodak Co., Rochester, NY, 2002, URL: http://www.kodak.com/ezpres/business/ccd/global/plugins/acrobat/en/datasheet/cmos/KAC-9628LongSpec.pdf , 2007.

31. Kodak datasheet, "KAC-01301 Product Summary," Eastman Kodak Co., Rochester, NY, URL: http://www.kodak.com/ezpres/business/ccd/global/plugins/acrobat/en/productsummary/CMOS/KAC-01301ProductSummaryv.1.0.pdf , 2007.

32. Janson, S.W., "Spacecraft As Assembly of ASIMs," in "*Microengineering Technology for Space Systems*," edited by H. Helvajian, p. 181-258, AIAA/Aerospace Press, October 1995.

33. Schneider, M. et al., "High Sensitivity CMOS MicroFluxgate Sensor," International Electron Devices Meeting Technical Digest, pp. 907-910, Washington D.C., Dec. 1997.

34. Wickenden, D.K., Givens, R.B., Osiander, R., Champion, J.L., Oursler, D.A. and Kistenmacher, T.J., "MEMS-based Resonating Xylophone Bar Magnetometer," Paper 3514-34, Proceedings SPIE Micromachined Devices and Components IV, Volume 3514, Santa Clara, CA, September 20-24, 1998.

35. Beroulle, V., Bertrand, Y., Latorre , L., and Nouet, P., "Micromachined CMOS Magnetic Field Sensors with Low-Noise Signal Conditioning," pp. 256-259, Proceedings of the 15th IEEE International Conference on Micro Electro Mechanical Systems, Las Vegas, NV, January 20-24, 2002.

36. Honeywell datasheet "1, 2 and 3 Axis Magnetic Sensors, HMC1051/HMC1052/HMC1053," Honeywell Solid State Electronics Center, Plymouth, MN, URL: http://www.ssec.honeywell.com/magnetic/datasheets/HMC105X.pdf , 2007.

37. Honeywell datasheet, "Three Axis magnetic Sensor Hybrid," Honeywell International Solid State Electronics Center, Plymouth, MN, URL: http://www.ssec.honeywell.com/magnetic/datasheets/hmc2003.pdf , 2007.

38. Analog Devices, ADIS16250/16255 programmable low power gyroscope data sheet, Analog Devices, Norwood, Massachusetts, URL: http://www.analog.com/UploadedFiles/Data_Sheets/ADIS16250_16255.pdf , 2007.

39. The MOSIS Service, "Welcome to MOSIS" Home Page, Marina del Rey, CA, URL: http://www.mosis.com//

40. Tanner Research, "MOSIS Mixed Signal Design Kits" page, Tanner EDA, Monrovia, CA, URL: http://www.tanner.com/EDA/product/designkits_MOSIS.html 2007.

41. Janson, Siegfried W, "Nanotechnology – Tools for the Satellite World," Keynote Address, 6th ISU Annual International Symposium; "Smaller Satellites, Bigger Business?", Strasbourg, France, 21-23 May, 2001, pp. 21-30, Kleuwer Acedemic, Norwell, MA, 2002.

42. Janson, Siegfried W., "Micro/Nanotechnology for Micro/Nano/Picosatellites," AIAA paper 2003-6269, 2003.

43. Lacoe, R.C. et al.: Application of Hardness-By-Design Methodology to Radiation-Tolerant ASIC Technologies, *IEEE Trans. On Nuclear Science, Vol. 47*, pp. 2334-2341, 2000.

44. Hales, J.H. and M. Pedersen, "Two-Axis MOEMS Sun Sensor for Picosatellites," 16th AIAA/USU Conf. On Small Satellites, paper SSC02-VI-6, 2002.

45. Bloom, A., "The Eagle Sun and Earth Sensors," Project Oscar 2004 Space Symposium, April 24, 2004, available on-line at: http://www.projectoscar.net/symposium/Alan_Bloom_Eagle.pdf?PHPSESSID=c49189c16d9325db18a9941379e707e4 2008.

46. AMSAT-ZL (New Zealand), "KiwiSAT, Sun Sensor," available on-line at: http://www.kiwisat.org.nz/sun_sensor.html 2008.

47. Hamamatsu Inc., "S7848 Series Datasheet," Hamamatsu City, Japan, available on-line at: http://sales.hamamatsu.com/assets/pdf/parts_S/S7848_series.pdf 2008.